Bulletin of Volcanology (2021) 83: 6
https://doi.org/10.1007/s00445-020-01427-y

RESEARCH ARTICLE

Formation of dense pyroclasts by sintering of ash particles during the preclimactic eruptions of Mt. Pinatubo in 1991

Yining Wang[1] · James E. Gardner[1] · Richard P. Hoblitt[2]

Received: 12 May 2020 / Accepted: 9 December 2020 / Published online: 13 January 2021

Abstract

Dense, vitric, dacitic pyroclasts (dacite lithics) from the 1991 preclimactic explosions of Mt. Pinatubo were analyzed for their vesicular and crystal textures and dissolved H_2O and CO_2 contents. Micron-scale heterogeneities in groundmass glass volatile contents (0.9 wt% differences in H_2O within 500 μm) are observed and argue that parts of the dacite lithics equilibrated at different depths before finally being constructed. Greater vesicularities and larger and greater number densities of vesicles are observed in groundmass glass around phenocrysts compared to groundmass glass away from phenocrysts, similar to textures produced in experiments that sintered bimodal distributions of particles. Furthermore, increasingly greater proportions of stretched and distorted vesicles are observed in lithics from the later explosions, which parallels the increasingly shorter reposes between explosions. Finally, micron-sized crystal fragments are ubiquitous in groundmass glass of all dacite lithics. The textures, together with the variable volatile contents, lead us to propose a model that the dacite lithics formed by rapid and repetitive sintering of ash particles derived from a variety of depths on the conduit walls above the fragmentation level. We speculate that sintering of conduit material produced impermeable layers that retarded gas flow through the conduit, causing pressure to build until the cap failed and the next explosion occurred.

Keywords Pumice · Lithic · Sinter · Explosive eruption · Mount Pinatubo

Introduction

Dense, juvenile magmatic fragments are common in tephra deposits and used to infer eruptive behavior and degassing processes (Eichelberger and Westrich 1981; Taylor et al. 1983; Newman et al. 1988; Bursik 1993; Rust et al. 2004; Gonnermann and Manga 2005a; Rust and Cashman 2007; Barnes et al. 2014; Gardner et al. 2017). Commonly, their volatile signatures appear to follow closed system degassing trends, but their poor vesicularities suggest various extents of gas escape, which should happen only in open-system degassing processes (Taylor et al. 1983; Newman et al. 1988; Rust et al. 2004; Castro et al. 2014; Watkins et al. 2017). Various models have been proposed to reconcile these contrasting records (Eichelberger et al. 1986; Rust et al. 2004; Gonnermann and Manga 2005a; Rust and Cashman 2007; Castro et al. 2014). Recently, Gardner et al. (2017) re-examined glassy obsidian pyroclasts from the 1325–1350 C.E. North Mono eruption and argued that the pyroclasts formed by repeated fragmentation and sintering of loose ash particles at various depths within the conduit. In this model, there is no need to reconcile degassing trends because dissolved volatile contents preserve degassing at various depths in the conduit but vesicles are mainly relict pockets of gas trapped between sintering ash and not those degassed from the local melt.

Although sintering serves as one model for the formation of glassy obsidian pyroclasts, it is not clear whether it occurs in non-obsidian forming eruptions. Therefore, in this study, we investigate the textures and volatile contents in dense, juvenile magmatic fragments erupted during a series of explosions before the climactic phase of the Mount Pinatubo eruption in 1991. As discussed below, these are phenocryst-rich, poorly vesicular fragments of the same dacite magma erupted

Editorial responsibility: S. Self; Deputy Executive Editor: J. Tadeucci

✉ James E. Gardner
gardner@jsg.utexas.edu

[1] Department of Geological Sciences, Jackson School of Geosciences, The University of Texas at Austin, Austin, TX 78712-0254, USA

[2] U.S. Geological Survey, Cascades Volcano Observatory, Vancouver, WA 98683-9589, USA

throughout the eruptive sequence. Hammer et al. (1999) showed the fragments formed during the explosions, which when paired with the well-documented eruptive durations and repose intervals, provides an excellent framework to study their formation. In this study, we refer to the vitric, dacitic, pyroclasts as dacite lithics to maintain consistency with Hoblitt et al. (1996), who described the deposits and the occurrence of the dacite lithics in detail. In addition, because viscous sintering is the same process as welding (e.g., Wadsworth et al. 2016, 2017a, 2017b), we refer to the process as sintering, which avoids any specific connotation of different degrees of welding as used in physical volcanology.

Background and samples

The reawakening of Mt. Pinatubo in 1991 began in March of that year with felt earthquakes and escalating steam and ash emissions (Wolfe and Hoblitt 1996). The emergence of a lava dome on June 7 (phase III, Hoblitt et al. 1996) provided proof that the activity was driven by ascending magma. Four powerful, vertical eruptions occurred during June 12–14 (phase IV), producing ash clouds that rose higher than 24 km and tephra fall that extended over wide areas. The pace of activity then quickened with thirteen closely spaced explosions during June 14–15 (phase V) that generated pyroclastic surges. These eruptions were transient, most lasting only a few minutes, and produced small volume deposits consisting of pyroclasts with variable density (Hoblitt et al. 1996), and thus can be considered Vulcanian-style eruptions (Clarke et al. 2015). The deposits are rich in pumiceous pyroclasts, suggesting the eruptions were magmatic rather than phreatomagmatic. While the intensity of the explosions generally decreased with time, they became more frequent (Table 1). Then, on June 15, about 5.5 km^3 (dense-rock equivalent) of pyroclastic material was emplaced during the climactic phase VI eruption (Hoblitt et al. 1996; Scott et al. 1996; Weisner et al. 2004).

The eruptive products consist of three major juvenile components: hybrid andesite (59–60 wt% SiO_2), olivine-clinopyroxene basalt (50–52 wt% SiO_2), and dacite (64.5 ± 0.3 wt% SiO_2; Pallister et al. 1996; Luhr and Melson 1996; Bernard et al. 1996). The climactic eruption tapped only dacite, which is volumetrically at least an order of magnitude greater than all deposits produced by the June 12–14 eruptions combined (Pallister et al. 1996). Phase IV activity, however, tapped 50–90 + % hybrid andesite (Hoblitt et al. 1996). The first explosion of phase V also erupted ~ 55% andesite, but tephra from the subsequent explosions is ~ 80–100% dacite.

Dacite clasts in phase V tephra are classified as either pumice or lithic (Fig. 1), with dacite lithics having densities ≥ 2000 kg m^{-3} (Table 1). Here, we focus on dacite lithics, which comprise 7–13% of dacitic material in deposits from surges 1 and 3, but make up ~ 40–50% of the later pyroclastic surge deposits (Hoblitt et al. 1996). We examined 48 dacite lithics (Table 1), all 2–10 mm in size, collected in March 1992 from site #11, located to the southeast of the caldera (Hoblitt et al. 1996). Eleven different pyroclastic surge deposits are thought to be present at that locality, and only 9 of those yielded sufficient deposit to be sampled. Three dacite pumice are included in the study for comparative purposes (Table 1).

Methods

Dacite lithics larger than 8 mm were broken into several pieces, and a select number were mounted in epoxy and doubly polished. Smaller lithics were doubly polished whole. Wafers were thinned to ~ 50–160-μm thick so that sufficient light could pass through the sample to facilitate measuring dissolved volatile contents in groundmass glass while avoiding phenocrysts, vesicles, microlites, and crystal fragments (Table 2).

Textural analysis

Textures were studied using a combination of scanning electron microscopy (SEM) and optical microscopy. A subset of 44 of the 48 samples were scanned using a Phillips/FEI XL30 environmental scanning electron microscope (The University of Texas at Austin) to produce back-scattered electrons (BSE) images and compositional X-ray maps. All image analyses were done using *AZtec* and *ImageJ*. The images were used to measure vesicularity, defined as the percentage of area of void space relative to the area of void space plus groundmass glass (minus crystals). Crystals were identified from stacked X-ray maps of Fe, Mg, Ca, Na, Al, P, Ti, and S. Crystallinity was calculated from the maps as the percentage of area of crystals relative to the total area of clast (minus vesicles). Groundmass glass abundances were then calculated by subtracting crystal and void areas from total area.

Except for three lithics that lack vesicles, sub-domains within each clast (typically 0.024 to 0.68 mm^2) with various vesicularity were selected randomly and measured for vesicularity. Each of those was then analyzed using an optical microscope to measure vesicle size, vesicle shape, and 3D vesicle number density. Vesicles in transparent groundmass glass were counted within rectangular columns in the selected subdomains as we focused through samples at a magnification of × 500. All vesicles were counted and measured as the focal plane traveled through the sample, until individual vesicles could no longer be identified. The distance that the focal plane traveled through the sample was measured using a linear drive encoder attached to the focusing drive of the microscope. Long and short axes of all identifiable vesicles were measured using the ocular reticle to a precision of 1 μm. Some vesicles are highly distorted, making long and short axes difficult to

Table 1 Chronology and samples of phase V eruptions of Mt. Pinatubo

Eruption date	Surge event	Previous repose (min)	Plume height (km)	Dacite in deposit (%)	Dacite lithics (%)	Samples (number)
6/14/91	1	124	?	58	12.9	7
6/14/91	2	210	≥24	–	–	0
6/14/91	3	262	21	98	6.7	8 (+2 dacite pumice)
6/15/91	4	112	?	87	44.2	4
6/15/91	5	79–99	?	85	48.8	4
6/15/91	6	174	12	80	38.5	1
6/15/91	7	132	12?	83	–	2
6/15/91	8	137	15?	82	–	5
6/15/91	9	36–46	?	98	–	12 (+1 dacite pumice)
6/15/91	10	28–37	8	100	–	5
6/15/91	11	15	?	–	–	0
6/15/91	12	20	?	–	–	0
6/15/91	13	19	?	–	–	0

Eruption data and percentages of dacite in each deposit from Hoblitt et al. (1996). "?" Heights were either not seen or roughly estimated. Percentages (by mass) of dacite lithics amongst dacite clasts are estimated from clast density distributions in Hoblitt et al. (1996). "–" no information provided

define; in those cases, the longest and shortest spans of vesicles were measured.

Glass composition

A total of 60 groundmass glasses were analyzed (Table 3) using a JEOL JXA-8200 Electron Microprobe (EPMA). One clast each from eight of the pyroclastic surge deposits was analyzed, and six to eleven spots were analyzed in each, all avoiding crystals and vesicles. An accelerating voltage of 15 kV, a beam current of 10 nA, and a defocused spot size of 10 μm were used to minimize Na migration. Automatic drift corrections were used on standard intensities, with working standards analyzed repeatedly to monitor for instrumental drift. Because of the presence of dissolved H_2O, concentrations of the major elements do not sum to 100 wt%; analyses are thus normalized to 100 wt%.

Volatile measurements

A total of 329 analyses of dissolved H_2O contents in groundmass glasses in 34 clasts were made using Fourier transform infrared (FTIR) spectroscopy (Table 2). Of those, 275 also yielded detectable amounts of dissolved CO_2. Spectra were obtained between 7800 and 650 cm^{-1} using 120 scans at a resolution of 4 cm^{-1}, a liquid-nitrogen-cooled detector, white light, KBr beamsplitter, and an aperture of 50 × 50 μm. At least 10 analyses were made in each lithic, selected so that measurements corresponded to various vesicle textures. Absorbances at ~5200 cm^{-1} (hydroxyl OH) and ~4500 cm^{-1} (molecular H_2O) were used to calculate dissolved H_2O contents, using the model of Zhang et al. (1997). Absorbance at ~2350 cm^{-1} was used to calculate CO_2 content, using a molar absorptivity of 1214 L cm^{-1} mol^{-1} (Behrens et al., 2004). Thickness for each spectrum was measured using the linear encoder, as described above.

Dacite pumice

Three pumice samples were analyzed to compare with the dacite lithics in terms of vesicle and crystal textures (Table 1). One sample in this study, P351, is the same one used by Hammer et al. (1999). It is mounted in epoxy and singly polished to a thickness ~30 μm. Vesicularity and mineralogy of crystal phases were analyzed using an optical microscope. The other two pumice clasts (from surge 3 and surge 9) were scanned using a high-resolution X-ray computed tomography at the University of Texas at 160 kV, 0.2 mA, with a voxel size of 9.6 μm. Images (16bit TIFF) were produced from each scan and used to conduct image analyses. These scans provided better results to evaluate 3D distributions of vesicles and crystals.

Results

Vesicle textures

Dacite lithics have bulk vesicularities from ~4 to ~55 vol%, except for one highly vesicular clast from the deposit of surge 9 that has 70 vol% vesicles (Supplemental Table A). In general, more vesicular clasts are more uniformly vesicular, but all clasts are texturally heterogeneous, with some parts being dense glass and other parts with up to ~65 vol% vesicles.

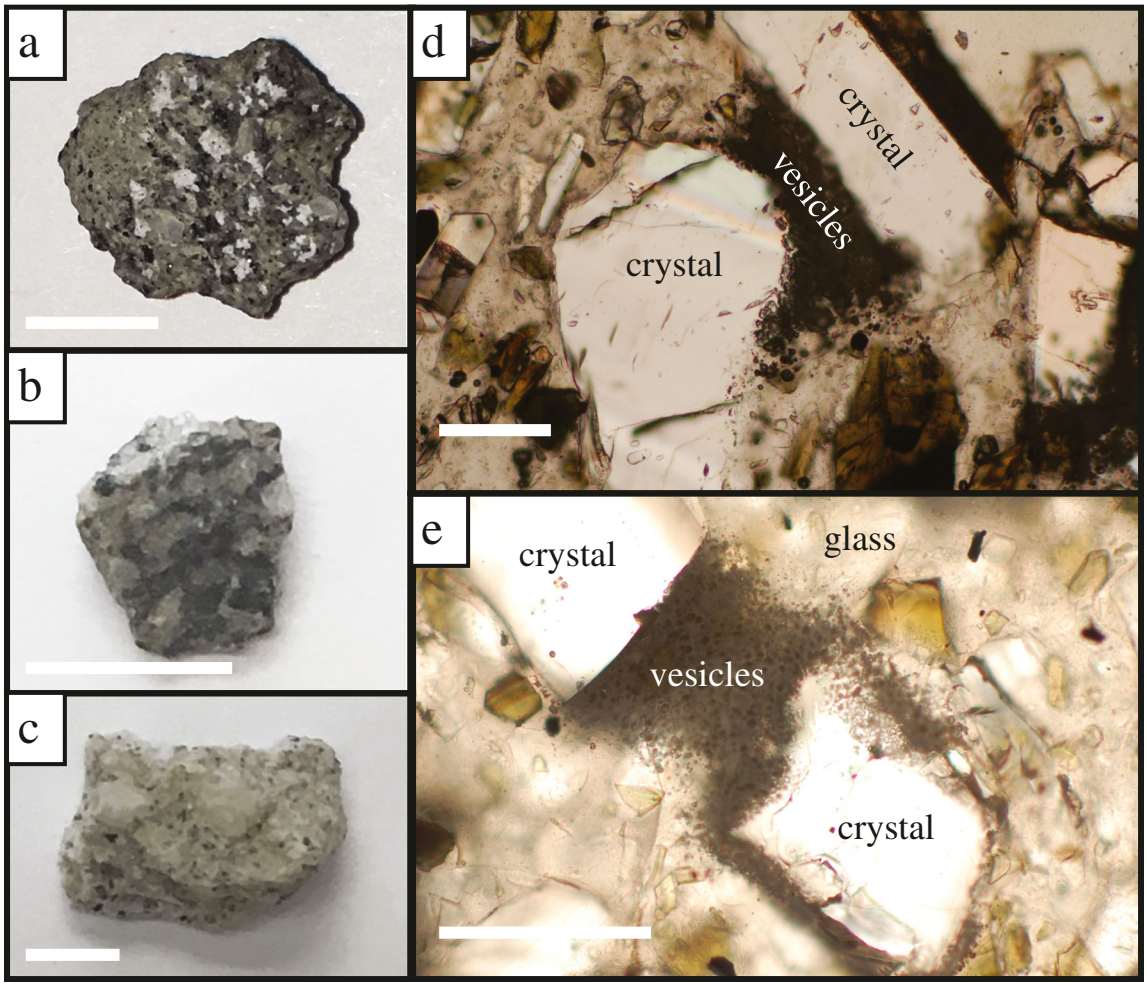

Fig. 1 Representative dacite lithics and pumice from the deposits produced from 1991 Mt. Pinatubo pyroclastic surges. **a** Dacite lithic from surge 9 deposit. **b** Dacite lithic from surge 1 deposit. **c** Dacite pumice from surge 1 deposit; all scale bars are 5 mm long. **d** and **e** Photomicrographs of heterogeneous vesicularities in dacite lithics; scale bars are 200 μm long. Note that highly vesicular pockets cluster around and between phenocrysts

Often, highly vesicular pockets are found next to and in between phenocrysts (Fig. 1). Greater vesicularities result from both greater numbers of vesicles and larger ones.

Vesicle shapes are classified following a scheme modified from that of Gardner et al. (2017). Vesicles are considered either regular or irregular (Fig. 2), and have either smooth

Table 2 Summary of volatile contents in dacite lithics of Mount Pinatubo

Surge event	*n* (H_2O)	[H_2O] average (wt%)	[H_2O] range (wt%)	*n* (CO_2)	[CO_2] average (ppm)	[CO_2] range (ppm)
1	9	1.3 ± 0.2	1.0–1.4	3	9 ± 2	7–10
3	73	1.6 ± 0.3	0.6–2.1	73	22 ± 5	9–35
4	36	1.8 ± 0.2	1.4–2.5	36	18 ± 5	10–27
5	30	1.8 ± 0.2	1.2–2.2	30	17 ± 4	11–29
6	10	1.6 ± 0.3	1.3–2.0	10	20 ± 4	13–27
8	32	1.6 ± 0.3	1.2–2.6	31	15 ± 7	5–30
9	82	1.5 ± 0.3	0.6–2.4	59	10 ± 4	4–22
10	54	1.4 ± 0.3	0.6–2.2	34	7 ± 1	4–11

n, total number of analyses from dacite lithics from each surge deposit. The average concentration of H_2O and CO_2 are listed in wt%, along with range between the lowest and highest concentration measured

Table 3 Average composition of groundmass glass in dacite lithics from Mt. Pinatubo surge deposits

Sample	1-1B	1-2B	1-3B	1-4B	1-5A	1-8C	1-9D	1-10B
Surge deposit	1	3	4	5	6	8	9	10
n	6	7	11	8	6	8	7	7
SiO_2	78.17 (42)	78.77 (21)	78.66 (24)	78.37 (17)	77.96 (62)	78.08 (26)	77.76 (28)	77.81 (38)
TiO_2	0.12 (3)	0.15 (5)	0.13 (3)	0.12 (4)	0.13 (3)	0.15 (2)	0.12 (2)	0.11 (3)
Al_2O_3	12.36 (14)	12.15 (19)	12.40 (16)	12.55 (13)	12.78 (42)	12.57 (8)	12.72 (10)	12.65 (19)
FeO*	0.84 (9)	0.84 (14)	0.75 (6)	0.73 (5)	0.71 (4)	0.82 (9)	0.78 (7)	0.80 (4)
MnO	0.03 (1)	0.04 (2)	0.03 (2)	0.03 (3)	0.05 (3)	0.03 (3)	0.03 (3)	0.04 (2)
MgO	0.22 (8)	0.17 (3)	0.18 (4)	0.18 (3)	0.11 (3)	0.19 (2)	0.22 (5)	0.23 (3)
CaO	1.11 (11)	1.02 (5)	1.04 (6)	1.05 (3)	1.19 (10)	1.08 (4)	1.15 (3)	1.19 (6)
Na_2O	4.04 (18)	3.61 (15)	3.65 (22)	3.88 (9)	4.05 (20)	4.00 (13)	4.12 (22)	4.04 (17)
K_2O	3.13 (6)	3.25 (3)	3.16 (12)	3.09 (8)	3.03 (16)	3.08 (7)	3.10 (5)	3.13 (8)

n, number of analyses. All oxides reported in weight percent and normalized to sum to 100%; total iron reported as FeO. Values in parentheses are 1σ standard deviations of concentrations in terms of the last digits of the average; 78.17 (42) should be read as 78.17 ± 0.42

surfaces or pitted and rough surfaces. We also classified vesicles using a dimensionless deformation parameter calculated from the vesicle dimensions:

$$D = \frac{l_a - l_b}{l_a + l_b} \quad (1)$$

where l_a and l_b are the lengths of the long and short axes (Taylor 1934; Rust and Manga 2002). Regularly shaped vesicles with D values of < 0.1 are considered spherical. Those with smooth surfaces are named "smooth spherical" (Fig. 2a), as opposed to those with rough surfaces, named "rough spherical" (Fig. 2b). Irregularly shaped vesicles that lack symmetrical shapes are classified as either "stretched-distorted," when they are elongated in one direction, or "distorted" when not (Fig. 2c). Regularly shaped vesicles with D values > 0.1 are ellipsoidal, and those can be either smooth (Fig. 2d) or rough, and in some cases have sharp tip(s) on one or both ends (Fig. 2e, f).

The most common vesicles are smooth spherical and smooth ellipsoidal. The proportion of smooth spherical vesicles within clasts ranges from 10 to ~ 80%, averaging 30 ± 14%. Smooth ellipses typically make up 20–65%, and average 40 ± 13%. Micron-scale heterogeneity of vesicle types occurs in most clasts, with stretched and sharp-tipped vesicles often found next to spherical and smooth ellipsoidal ones (Fig. 2d).

Dacite lithics from individual pyroclastic surge deposits can differ significantly in the dominant vesicle shapes within them. For example, one clast from the surge 4 deposit contains 44% distorted vesicles, whereas another from the same deposit lacks distorted vesicles and instead has nearly equal proportions of spherical and ellipsoidal vesicles. There are, however, systematic changes in vesicle textures through the sequence of layers. Sharp-tipped and stretched distorted vesicles are nearly absent in clasts from the earliest surge deposits, whereas both types are abundant in clasts from the deposits of surges 9 and 10 (Fig. 2e, f). Other vesicles generally become more stretched with time. Almost all vesicles in clasts from deposits of surges 1–7 have average D values of < 0.16, but they have average D values of > 0.16 in about half of the clasts from deposits of surges 8 and 9; 80% of the clasts from the deposit of surge 10 have average D value ≥ 0.2. In addition, whereas larger vesicles tend to be more deformed than smaller ones in most clasts, even many of the small vesicles in clasts from the deposit of surge 10 are stretched and distorted. Rough textured vesicles are also common in clasts from the deposit of surge 9, but uncommon in most other layers.

Dissolved volatile contents

The average H_2O and CO_2 contents in the 34 dacite lithics are 1.56 ± 0.21 wt% and 14.2 ± 2.9 ppm, respectively (Table 2). Individual analyses of H_2O concentrations range from 0.56 to 2.58 wt%, whereas CO_2 concentrations range from 4 to 35 ppm, when there is detectable CO_2 (Supplemental Table A). These concentrations overlap with those reported by Hammer et al. (1999).

Within clasts, concentrations of H_2O and CO_2 vary by up to ~ 1.3 wt% and ~ 18 ppm, respectively (Table 2). Intra-clast variations are typically much less than inter-clast variations. For example, clast 1–2L–B (from surge 3) has average concentrations of H_2O and CO_2 of 1.30 ± 0.53 wt% and 19 ± 5 ppm, respectively, which match averages for all clasts. Within that clast, however, groundmass glass in one area has 0.59 wt% H_2O and 12 ppm CO_2, whereas glass only 500 μm away contains 1.49 wt% H_2O and 22 ppm CO_2.

Overall, average H_2O concentrations fall within the range of 1–2 wt%, and clasts within the deposit of an individual pyroclastic surge event do not differ by more

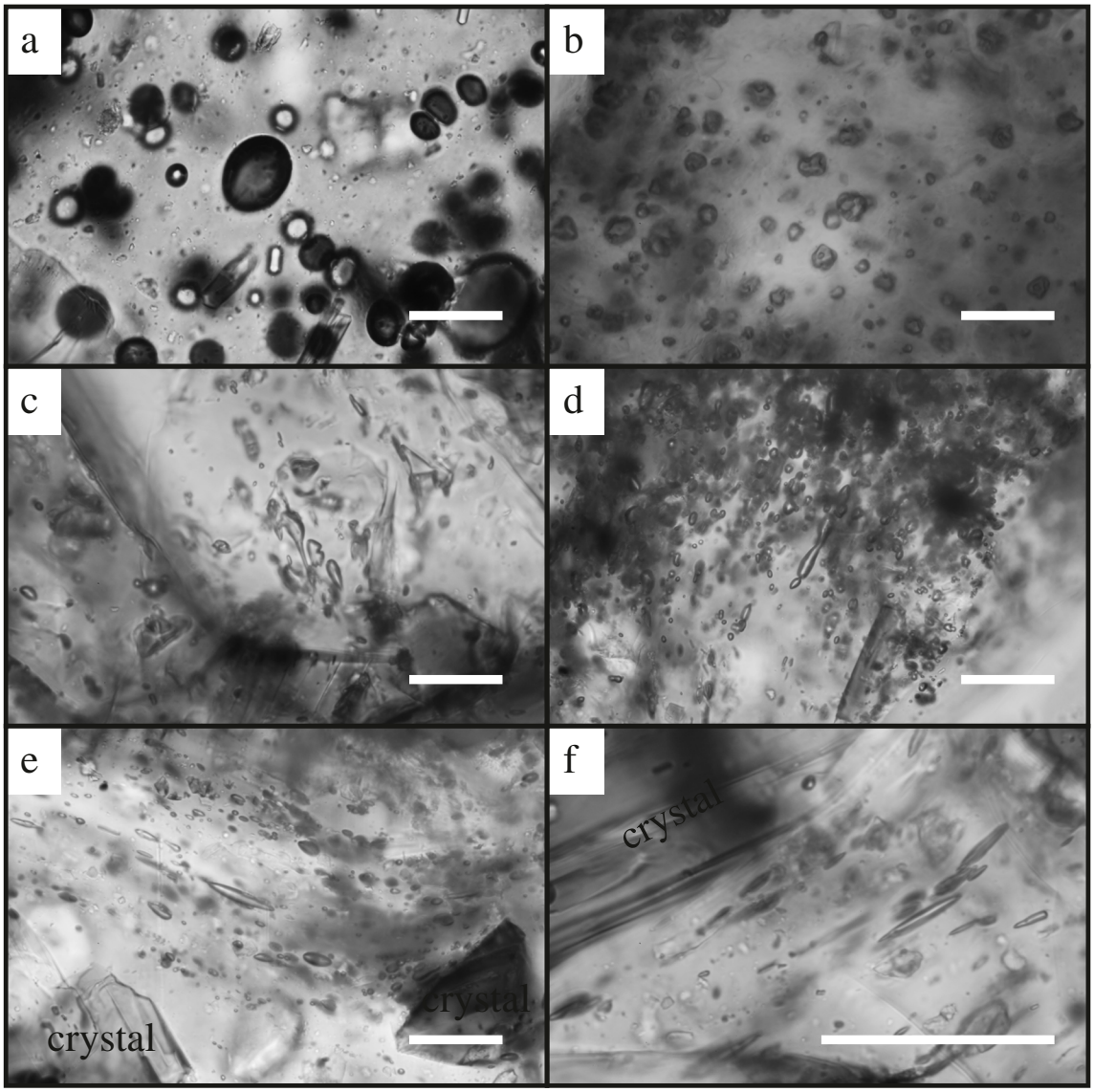

Fig. 2 Photomicrographs of vesicles textures observed in dacite lithics from deposits produced from the 1991 Mt. Pinatubo pyroclastic surges. **a** Homogeneously distributed smooth spherical vesicles in sample 1–8A (surge 8). **b** Rough spherical vesicles in sample 1-2L-C (surge 3). **c** Stretched distorted vesicle in a context with various degrees of vesicle relaxation in sample 1-10A (surge 10). **d** Smooth ellipsoidal and smooth spherical vesicles in sample 1–8A (surge 8). **e** Sharp-tipped ellipsoidal and distorted vesicles in sample 1-10A (surge 10). **f** Sharp-tipped ellipsoidal vesicles in sheared context from surge 10 samples. All scale bars are 50-μm long

than 0.7 wt% (Fig. 3). Differences in average CO_2 concentration amongst clasts from an individual pyroclastic surge event are also relatively small, usually below 10 ppm. But, there is a significant decrease in the average CO_2 concentration with time, decreasing from ~ 22 ppm in clasts from the deposit of surge 3 to < 7 ppm in clasts from the deposit of surge 10 (Fig. 3). The trend is significant because all 59 analyses in clasts from surge 9 are below 22 ppm. Clasts from surge 10 deposit have highly clustered dissolved CO_2 concentrations of ~ 5 and ~ 10 ppm. Clasts from surge 1 deposit are also poor in CO_2, but the limited number (3) of analyses makes the average suspect.

Crystals and crystal fragments

Bulk crystallinity of the dacite lithics ranges from ~ 40 to ~ 60 vol% (Supplemental Table A). The majority of the crystallinity are phenocrysts, up to ~ 2 mm in size, of feldspar (15–20 vol%), hornblende and cummingtonite (15–20 vol%), quartz (0–10 vol%), and minor amounts of biotite (up to 5 modal %), apatite (<5 vol%), and Fe–Ti oxides (~ 5 vol%). Microlites like those described by Hammer et al. (1999) are also observed (Fig. 4). Microlites larger than 150 μm are common in dacite lithics from the surge 1 deposit, and typically tabular in shape with slightly curved edges. Feldspar microlites shorter than 5 μm are observed in clasts from deposits of

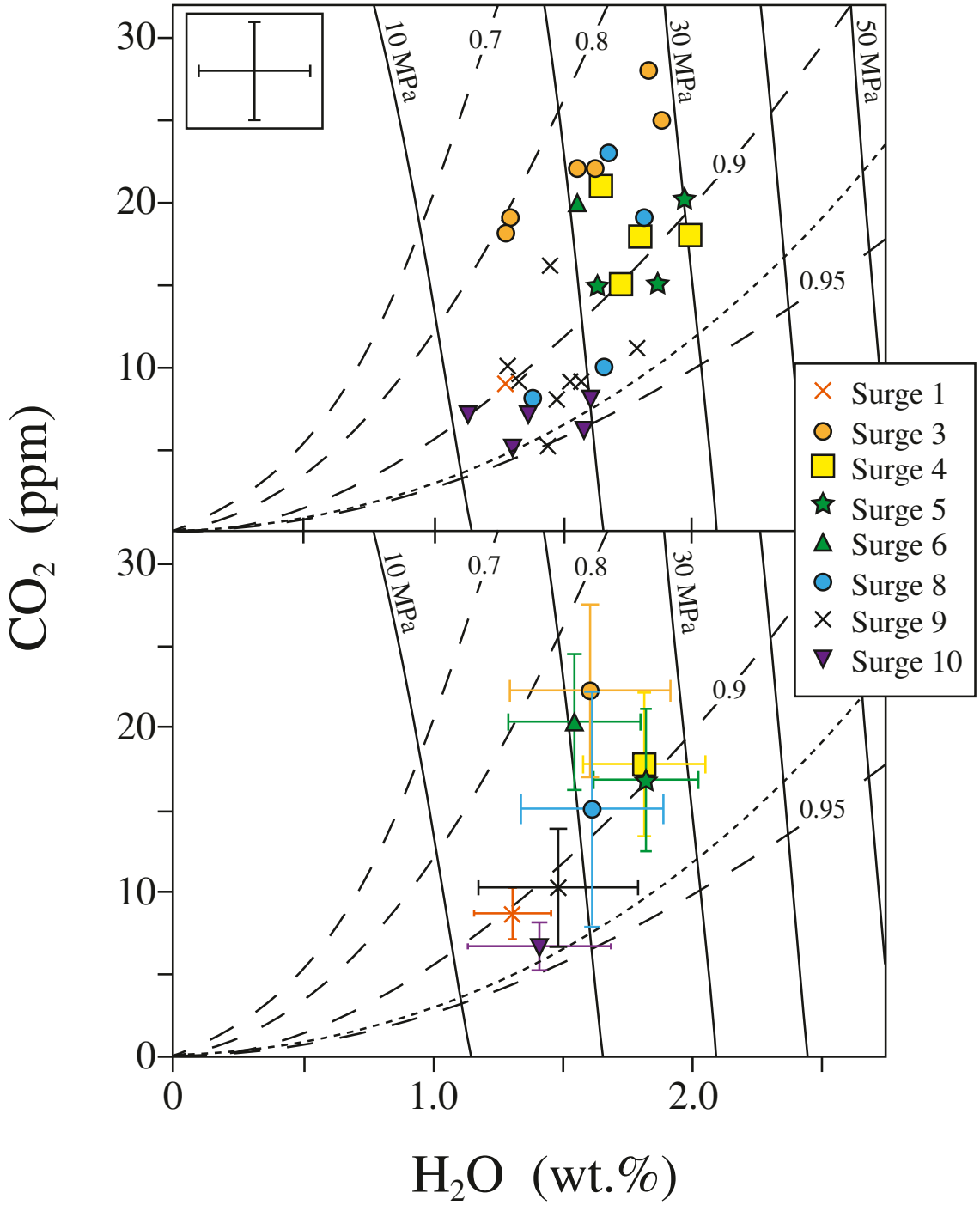

Fig. 3 (A) Average concentrations of dissolved volatiles in dacite lithics from 1991 Mt. Pinatubo pyroclastic surge deposits. Each datum represents the average volatile content of a sample; the average error is shown separately as bars at the top-left corner. (B) Average concentrations of dissolved volatiles for samples from each pyroclastic surge deposit. Error bars are ±1σ for all analyses. Solid and dashed curves in each figure are equilibrium volatile pressures and fluid compositions, respectively, calculated using the model of Liu et al. (2005) and assuming a magmatic temperature of 780 °C. Dotted curves are degassing paths calculated assuming closed system degassing of 6.3 wt% H_2O and 330 ppm CO_2 at 780 °C (Wallace and Gerlach 1994)

surges 4 and 5, with some having swallow-tailed offshoots, and show no preferred orientation in matrix glass. Microlites are essentially absent in lithics from deposits of surges 9 and 10. There is thus a systematic decrease in abundance and size of microlites as a function of time, a trend also observed and discussed in detail by Hammer et al. (1999).

In addition to well-shaped microlites, we observed numerous tiny fragments of crystals in every lithic (Fig. 4).

These ubiquitous fragments are randomly distributed throughout the groundmass glass and usually only a few microns in size, but some can be as big as 10–20 μm. They typically bear no crystal habit, which distinguishes them from microlites, yet they have sharp edges regardless of size. The most abundant fragments are colorless feldspar and pale green hornblende, and are thus the same as the phenocryst population.

Dacite pumice

Pumice sample (P351) from the deposit of surge 3 is highly vesicular, with clear groundmass glass that is free of microlites and crystal fragments (Fig. 4). Vesicles and phenocrysts make up ~40 vol% and ~50 vol% of the pumice, respectively. The other pumices from the deposits of surge 3 (P1-2A) and surge 9 (P1-9A) have similar crystallinities of 40–50%. Phenocryst phases observed include feldspar, hornblende, and quartz. These pumice clasts match the phenocryst-rich pumice found in phase VI deposits. Hoblitt et al. (1996) noted that the phase V deposits lack crystal fragment–rich tan pumice, which are common in phase VI deposits.

Discussion

Source of dacite lithics

Groundmass glasses in eight dacite lithics, one from each of the surge deposits, are all high-silica rhyolitic in composition (Table 3), and match the composition of glass in the dacite magma erupted during phase VI (Rutherford and Devine 1996; Pallister et al. 1996). All dacite lithics have phenocrysts that are found only in the main dacite magma; no crystals from the hybrid andesite or olivine-clinopyroxene basalt were observed. We conclude that all dacite lithics examined are dacite only, and hence none of the textures can be ascribed to magma mixing.

Dacite lithics were erupted in a sequence of explosions that lasted for nearly 24 h (Wolfe and Hoblitt 1996). Hammer et al. (1999) found that well-formed microlites in the lithics vary in size and number between explosions, but are absent from the main dacite magma erupted during the climactic phase VI event. We also found that microlites are absent from dacite pumice erupted by the phase V explosions (Fig. 4). This argues that the dacite lithics formed during the sequence of explosions, and hence in less than ~24 h. More importantly, sizes and abundances of microlites correlate roughly with length of repose, suggesting that the lithics formed during

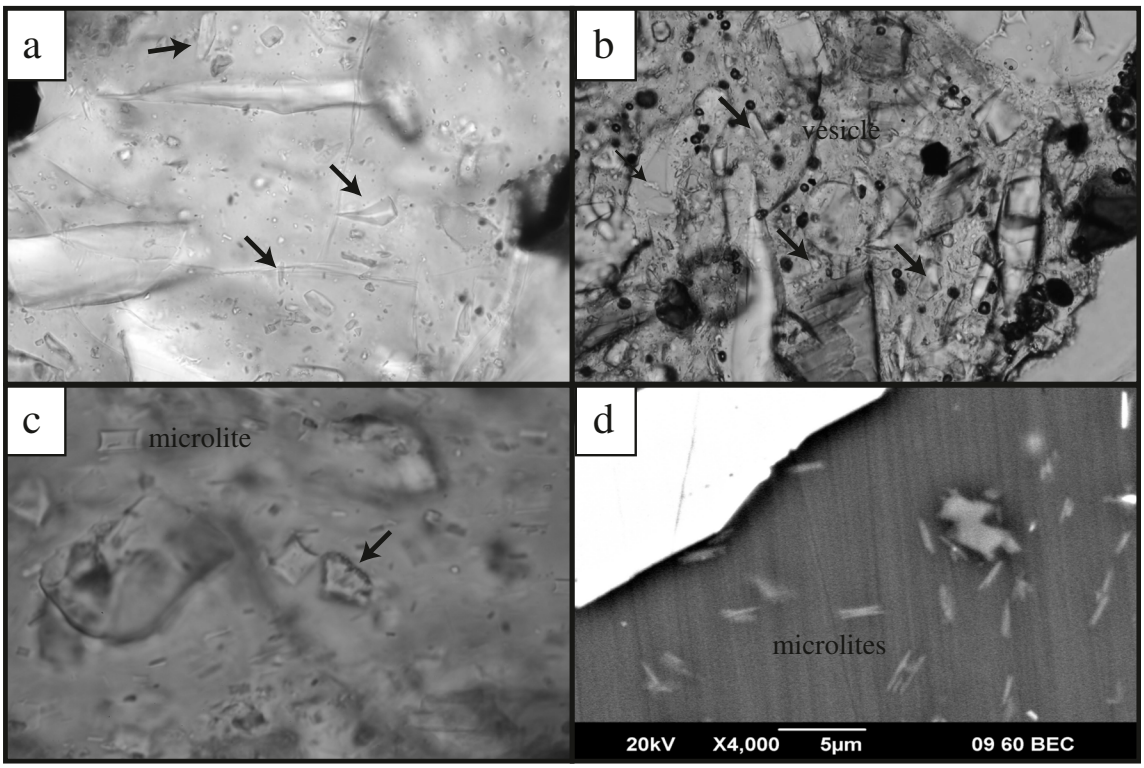

Fig. 4 Optical microscope (**a–c**) and SEM images (**d**) of crystal fragments (**a–c**) and microlites (**d**) in 1991 Mt. Pinatubo dacite lithics. Arrows point to crystal fragments. Clasts are from pyroclastic surge deposits produced by surges 10, 8, 1, and 5, respectively

reposes between explosions (Hammer et al. 1999). Reposes between the earliest explosions lasted up to 2 h, but decreased to about 20 min by the end of the sequence (Table 1). Such a correlation would not be expected if the dacite lithics were not formed during the sequence of eruptions and instead were accidental lithic fragments of pre-existing rocks.

Dissolved volatile contents are mainly 1–2 wt% H_2O and 5–30 ppm CO_2 (Fig. 3). If equilibrium conditions are assumed, the dacite lithics formed at ~ 11 to 30 MPa, as calculated from the model of Liu et al. (2005). These are significantly lower than the pre-eruptive pressures of the dacite magma (Wallace and Gerlach 1994; Rutherford and Devine 1996).

The magma that produced the dacite lithics thus formed within relatively short time periods and at shallow depths rather than within the pre-eruptive magma reservoir. We note that if H_2O-rich dacite magma degassed from 220 MPa (pre-eruptive magma reservoir) to 11–30 MPa, then it would have generated porosities of ~ 65–78 vol% (Gardner et al. 1999). The dacite lithics are far less porous, however, and in fact many have nearly bubble-free groundmasses (Figs. 2 and 4). Thus, a significant loss of porosity must have occurred during the minutes to hours while the dense dacite formed. One possibility is that the highly porous magma stagnated long enough for bubbles to interconnect and form a permeable foam that allowed gas to escape and the foam to subsequently collapse as a result of surface tension (Eichelberger et al. 1986). The main control on the rate of foam collapse in the absence of applied stress is the viscosity of the porous melt (Proussevitch et al. 1993; Gardner et al., 1996; Martel and Iacono-Marziano 2015). Using the model of Hess and Dingwell (1996), we estimate that the silicate melt (groundmass glass) of the dacite lithics would have had viscosities of $10^{6.1}$–$10^{8.5}$ Pa s, using measured H_2O contents (Table 2), measured glass compositions (Table 3), and a temperature of 780 °C (Rutherford and Devine 1996; Scaillet and Evans 1999). Bulk viscosity would have been higher, because of the presence of ~ 40–60 vol% phenocrysts (Table 2). Even assuming melt viscosity alone, the experimental results of Martel and Iacono-Marziano (2015) indicate that such foam would take more than 10^4 h to collapse. Moreover, as discussed by Wadsworth et al. (2020), densification of foam is limited to 20–30 vol% porosity, because of the collapse of the permeable network, and even when magmatic foams have been sheared experimentally, the lowest porosity achieved has been 17 vol%. Many of the dacite lithics are less vesicular than 17–20 vol%, including many that have groundmasses with near zero vesicularity. It thus seems unlikely that that the dense dacite formed solely as a result of collapse of permeable foam at shallow depths.

Generation of dacite lithics after fragmentation

One key to understanding how the dense dacite formed is the ubiquitous fragments of crystals (Fig. 4). Such fragments are absent from the groundmass glass in dacite pumice (Fig. 4d), but are found in every dacite lithic, including those that lack microlites (Fig. 4). The fragments match the phenocryst population, but their shapes and textures show they are not microlites grown from the melt. Importantly, amphibole fragments are common, but hornblende would not grow from melt with only 1–2 wt% dissolved H_2O (Rutherford and Devine 1996; Browne and Gardner 2006). Hence, the fragments are inherent to the dense dacite, but they did not grow from the melt at the conditions recorded by the dacite lithics.

Similar small pieces of crystals were observed in gray pumice erupted in phase VI (Pallister et al. 1996; Polacci et al. 2001). These crystal pieces coincide with a dramatic decrease in phenocryst abundance of up to 15% or more, and with distinctly more mafic groundmass glass, with SiO_2 contents as low as 68 wt% (Bernard et al. 1996; Luhr and Melson 1996; Pallister et al. 1996; Scaillet and Evans 1999). Like the white pumice clasts, however, gray pumice clasts are highly vesicular, with bulk vesicularities of 68–72% (Polacci et al. 2001). Polacci et al. (2001) argue that these crystal pieces formed by mechanical breakage and dissolution of phenocrysts as a result of intense shear and viscous dissipation at the conduit walls during ascent in the conduit before the magma fragmented into pumice and ash.

Gray dacite pumice makes up ~ 15% of phase VI deposits, in contrast to dacite lithics which make up almost half of some of the deposits of phase V (Hoblitt et al. 1996). Dacite lithics also have the same modal abundances of phenocrysts as white pumice (Table 2) and there is no change in groundmass glass composition (Table 3). This shows conclusively that the crystal fragments in the dense dacite did not result from phenocryst dissolution. In addition, vesicularities of dacite lithics are highly variable, and in some cases are almost non-vesicular. The groundmass glasses of dacite lithics are also highly variable in dissolved volatile contents, which would not be expected from degassing of a coherent, non-fragmented mass of magma. Finally, microlite contents and sizes in dacite lithics correlate with the length of hiatus between eruptions (Hammer et al. 1999), which would not be expected if the dacite lithics formed by shear during the eruptions. We thus argue that the dacite lithics are not the equivalent of the gray dacite and formed by a different mechanism.

The lack of crystal habit but sharp edges indicates the fragments formed by mechanical attrition and/or abrasion of phenocrysts. But, the fragments are randomly dispersed and not restricted to being near phenocrysts of similar type, e.g., feldspar fragments are found in between amphibole phenocrysts, and all types of fragments are found between phenocrysts of a single type. In order for the fragments to be randomly

dispersed, they must have been free from the groundmass after being broken off of phenocrysts. We thus argue that phenocrysts of the dacite magma were freed from the magma, broken and abraded to produce fragments, and then both the phenocrysts and fragments were re-incorporated into the magma. Because it is unlikely that individual phenocrysts can be released from the magma without the melt/glass also being dispersed, we suggest that the crystal fragments preserve a record of the dacite magma having been fragmented apart before the dacite lithics formed and erupted at the vent.

Model for the formation of dacite lithics

Our model for the formation of dacite lithics, following Wadsworth et al. (2020), starts with fragmentation of rising magma, which ultimately drives the eruptions (Fig. 5). The magma is fragmented into molten pumice, ash, and phenocrysts, and those free phenocrysts further break and abrade to produce the crystal fragments. As the fragmented mixture travels up the conduit some of the molten ash impacts and sticks to the conduit walls (Wadsworth et al. 2020), along with phenocrysts and crystal fragments. Continued eruption plasters more ash onto the aggrading material along the walls. That molten mass then sinters together, forming dense dacite. Pieces of the sintering mass are then fractured off and incorporated into the eruptions, similar to the ability of eruptions to incorporate accidental lithics from conduit walls (Gardner et al. 2017). Pieces fractured off of the conduit walls are either recaptured higher up in the conduit or ultimately expelled out of the conduit as dacite lithics (Fig. 5).

In order for ash sintering to be a viable mechanism to form dense dacite, it must operate on timescales comparable to the reposes between explosions. Gardner et al. (2018, 2019) experimentally sintered ash-sized rhyolitic glass at similar temperatures (700–800 °C) as the Pinatubo dacite (Rutherford and Devine 1996; Scaillet and Evans 1999) and H_2O contents and pressures (20–40 MPa) as those of the dacite lithics (Table 2). Loose ash was found to sinter to solid glass with few, spherical vesicles in tens of minutes to hours, depending on melt viscosity and particle size. It should be noted that sintering in those experiments occurred in the absence of any applied stress, and so those times can be considered maxima. Importantly, sintering of fine ash at 750 °C generated dense glass in ~ 10 min, which is comparable to the shortest reposes (Table 1).

Textural record of sintering to form dacite lithics

We propose that the dacite lithics were produced by sintering of fragmented dacite magma along the conduit walls during and between explosions (Fig. 5). In this model, textural variations amongst the clasts result from variable times allowed for sintering, and variable viscosities resulting from different H_2O contents (Table 2). Volatile contents within individual dacite clasts are highly variable, differing by as much as ~ 1 wt% H_2O (Table 2). In our model, such heterogeneities result from sintering particles that had previously degassed at different depths (pressures). The observed heterogeneities argue for relatively short times for formation, because H_2O diffusion would reduce any gradients. Watkins et al. (2017), for example, showed that volatile gradients within obsidian pyroclasts reflect re-equilibrations on order of a few hours. Interestingly, they derived diffusive times of ~ 2 h (assuming 800 °C) for H_2O and CO_2 gradients from 1.35 to 1.55 wt% and 22 to 29 ppm, respectively, spread across ~ 1000 μm. We found in one dacite lithic variations in H_2O and CO_2 of 0.90 wt% and 10 ppm, respectively, separated by only 500 μm. These argue that glass domains within the lithic could have co-existed for only a short period of time, similar to the repose periods (Table 1).

Within our framework, some, if not most, vesicles in the dense clasts are remnants of sutures between sintered particles. Initially, such pore space would be connected and highly irregular in shape, but as sintering proceeds and gas escapes, the pores relax in shape, resulting in spherical vesicles (Gardner et al. 2017, 2018). The rate of relaxation is controlled by melt viscosity and particle size, and so the variability in vesicle shapes within the dacite lithics could reflect sintering of various sized particles with different H_2O contents (i.e., different viscosities).

Stretched vesicles (i.e., stretched distorted, sharp-tipped ellipsoidal) are more abundant in dacite lithics from deposits of surge 9 and especially surge 10 (Fig. 2e, f). Those explosions followed short reposes (Table 1). Dacite lithics from earlier explosions, which followed longer reposes (Table 1), have more smooth spherical and smooth ellipsoidal ones. It is likely that stretched vesicles record deformation of the sintering mass while being re-incorporated into the erupting mixture (Fig. 5). On the other hand, relatively relaxed vesicles (spherical and smooth ellipsoidal vesicles) occur very close to sharp-tipped ellipsoidal vesicles and are the most abundant vesicles in all dacite lithics. If vesicle shapes solely resulted from re-mobilization of the magma back into the eruption mixture, then we would expect all vesicles within a dacite lithic to reflect the same degree of stretching, and not find highly stretched vesicles adjacent to spherical ones. We thus speculate that the vesicle heterogeneities mimic volatile heterogeneities, with each dacite lithic being the conglomeration of sintered masses, each of which experienced different histories of sintering and deformation.

One vesicle texture seen in dacite lithics that differs from obsidian pyroclasts (Gardner et al. 2017) is the strongly heterogeneous abundance of vesicles and highly vesicular domains around and between large phenocrysts (Fig. 1). Such heterogeneities were, however, produced in recent sintering experiments that used strongly bimodal mixtures of fine and

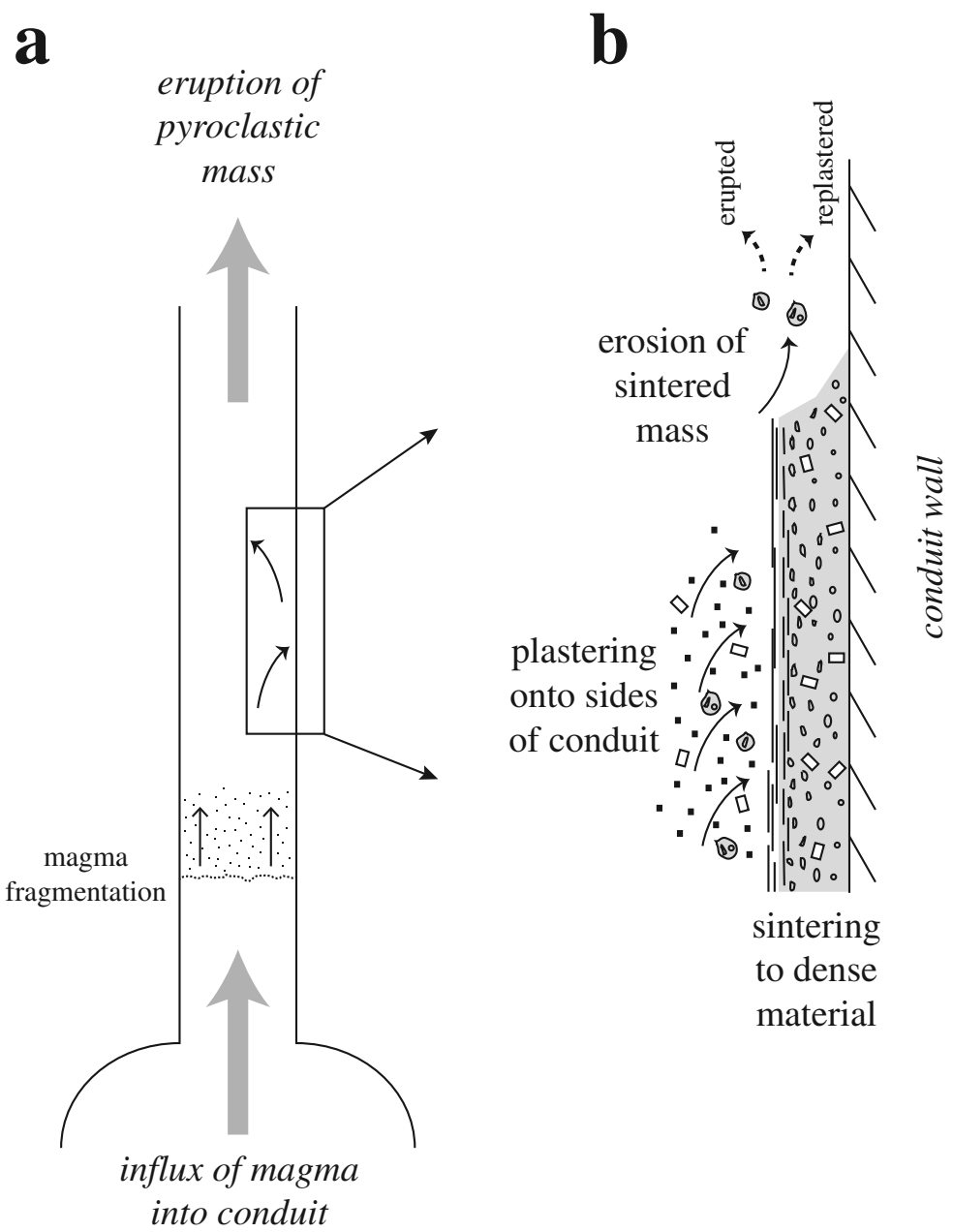

Fig. 5 Schematic model for the production and eruption of dacite lithics. **a** Magma rising into the conduit fragments at depth into a turbulent mixture of pumice, ash, and crystals. Small crystal fragments are generated from phenocrysts being broken and abraded. **b** Turbulently rising pyroclastic material hits and adheres to the conduit walls, where it sinters together into a dense dacite mass. That layer builds by continued plastering of new material, and is eroded by the eruption. Pieces of the dacite mass eroded from the sintered mass either erupt as dacite lithics or re-adhere along the walls. Note that pieces can be eroded and re-adhere multiple times, resulting in dacite lithics that have sub-domains that experienced complex and contrasting histories

coarse rhyolitic glass particles (Gardner et al. 2019). After about 20 min of sintering, the samples consisted of glass with ~ 3 vol% vesicles, except near and especially in between relict coarse particles, where the matrix contained up to 30 vol% vesicles. The coarse glass first acted like rigid bodies, preventing the surrounding matrix from sintering, but eventually deformed viscously after 30–45 min. Phenocrysts would instead remain rigid.

Implications for the volcanic eruptions

During many of the phase V explosions, the amount of dacite lithics erupted was up to half of the tephra (Table 1). It is possible that enough dense magma formed to make a relatively impermeable layer that clogged the conduit (e.g., Wright et al. 2007; Kolzenburg et al. 2019). In that case, gas flux through the conduit would be restricted, causing pressure to build until the cap failed, leading to the next explosion. Sintering within volcanic conduits may thus be one mechanism to facilitate similar Vulcanian-style explosions, which are thought to result from rapid decompression of pressurized magma (Self et al. 1979; Woods 1995; Clarke et al. 2015). Wright et al. (2007) argue that densification of upper conduit magma allows re-pressurization between explosions, and sintering would be one mechanism by which densification could occur on the short timescales of the phase V explosions. Hoblitt et al. (1996) suggested that vent clogging as a result of degassing

led to the decline in the eruptive vigor of the preclimactic eruptions.

Volatile contents in the dacite lithics range between ~ 1–2 wt% H_2O and 5–30 ppm CO_2 (Fig. 3). These contents overlap those found in other dense pyroclasts (Newman et al. 1988; Rust et al. 2004; Rust and Cashman 2007; Gardner et al. 2017). It is possible that this range of volatile contents represents optimal conditions needed for ash to sinter together yet and still be re-incorporated into an explosive event. Sintering of ash with lower H_2O contents takes longer, because of the higher melt viscosity (Gardner et al. 2018), which makes it less likely that dense material can form before being sheared off the walls. Less intense sintering would also generate more fragile particles that would easily fall apart under stress (Gardner et al. 2018). At the other end, higher H_2O contents may not be possible as they would exceed those expected to still be dissolved in magma when it fragments to generate ash particles. The range of volatile contents preserved in dense pyroclasts could thus represent sintering efficiency and clast preservation rather than degassing behavior.

Although the average dissolved H_2O concentration was relatively steady at 1–2 wt% during the sequence of explosions in phase V, dissolved CO_2 concentrations decreased by a factor of two, resulting in a decrease in the CO_2/H_2O ratio with time (Fig. 3). Neither closed nor open system degassing models can explain such a difference in CO_2/H_2O at similar H_2O contents (Fig. 3). Similar variations have been reported in other dense pyroclasts (Newman et al. 1988; Rust et al. 2004; Rust and Cashman 2007; Gardner et al. 2017). Gonnermann and Manga (2005b) argued that variations in CO_2/H_2O arise from the slower diffusivity of CO_2, with shorter degassing times giving rise to higher CO_2/H_2O ratios because of the preferential loss of H_2O. In the case of the Pinatubo eruptions, however, the decrease in CO_2/H_2O ratio correlates with shorter repose periods, and presumably less time for diffusion. Non-equilibrium degassing does not seem viable to explain the change in CO_2/H_2O. Rust and Cashman (2007) argued that incorporation of xenolithic material could influx CO_2 into the magma, causing shifts in CO_2/H_2O. There is, however, no evidence for xenolithic material in the Pinatubo dacite lithics, and so it is not possible for such material to be a source of CO_2. We propose instead that the trend of decreasing CO_2/H_2O with time reflects the amounts of CO_2 fluid released from the basaltic magma that had intruded into the dacitic magma (Pallister et al. 1992, 1996). Because the amount of mafic magma decreased during the eruption series (Hoblitt et al. 1996), the amount of CO_2 released decreased with time as well.

Conclusions

Dacite lithics from the 1991 preclimactic eruptions of Mt. Pinatubo provide a window into syn-eruptive conduit dynamics. Ubiquitous micron-sized crystal fragments in the dacite lithics requires that the erupting magma fragmented into ash and phenocrysts in the conduit, and then some of which was sintered back together into coherent material. Significant variations in volatile contents across short distances and the existence of highly deformed vesicles argue that the timescales for sintering were short, and probably on order of the tens of minutes of repose that separated the explosions. This model is consistent with that of Hammer et al. (1999), who argued, based on the general correlation of microlite sizes and abundances with repose times, that the dense dacite magma formed during the repose periods. Later erupted dacite lithics have more deformed and stretched vesicles, possibly reflecting the decreased amounts of time for assembly and relaxation of the sintering material. Shorter times are supported by the general lack of microlites in the later erupted dacite lithics (Hammer et al. 1999). Dissolved volatile contents in the groundmass glasses indicate that sintering took place mainly at pressures of 11–30 MPa. Continued sintering of material at these shallow levels in the conduit may have developed an impervious cap that allowed pressure to build, leading to the next Vulcanian-style explosion. Dissolved CO_2 contents decreased significantly with time and probably reflect the waning input of CO_2 fluid released from basaltic magma that had been injected into the resident dacite magma at depth that reawakened the magmatic system (Pallister et al. 1992).

Supplementary Information The online version contains supplementary material available at https://doi.org/10.1007/s00445-020-01427-y.

Acknowledgments The authors thank E. Llewellin and F. Wadsworth for discussions on sintering processes; J. Manor for assistance with scanning electron microprobe analyses; and J. Maisano for collection and analysis of HRXCT data. The manuscript was improved greatly from an internal US Geological Survey review by Dr. John Pallister and reviews by Steve Quane and Mike Branney. The authors acknowledge support from the National Science Foundation from grant EAR–1725186 to JEG. Any use of trade, firm, or product names is for descriptive purposes only and does not imply endorsement by the US Government.

References

Barnes JD, Prather TJ, Cisneros M, Befus K, Gardner JE, Larson TE (2014) Stable chlorine isotope behavior during volcanic degassing of H2O and CO2 at mono craters, CA. Bull Volcanol 76(3)

Bernard A, Knittel U, Weber B, Weis D, Albrecht A, Hattori K, Oles D (1996) Petrology and geochemistry of the 1991 eruption products of Mount Pinatubo. Fire and mud: eruptions and lahars of Mount Pinatubo, Philippines, pp 767–797

Browne BL, Gardner JE (2006) The influence of magma ascent path on the texture, mineralogy, and formation of hornblende reaction rims. Earth Planet Sci Lett 246:161–176

Bursik M (1993) Subplinian eruption mechanisms inferred from volatile and clast dispersal data. J Volcanol Geotherm Res 57:57–70

Castro JM, Bindeman IN, Tuffen H, Schipper CI (2014) Explosive origin of silicic lava: textural and –H2O evidence for pyroclastic degassing during rhyolite effusion. Earth Planet Sci Lett 405:52–61

Clarke AM, Esposti Ongaro T, Belousov A (2015) Vulcanian eruptions. In: Sigurdsson H, Hougton B, McNutt SR, Rymer H, Stix J (eds) Encyclopedia of Volcanoes, 2nd edn. Acad Press, London, pp 505–518

Eichelberger JC, Westrich HR (1981) Magmatic volatiles in explosive rhyolitic eruptions. Geophys Res Lett 8:757–760

Eichelberger JC, Carrigan CR, Westrich HR, Price RH (1986) Non-explosive silicic volcanism. Nature 323(6089):598–602

Gardner JE, Hilton M, Carroll MR (1999) Experimental constraints on degassing of magma: isothermal bubble growth during continuous decompression from high pressure. Earth Planet Sci Lett 168(1–2): 201–218

Gardner JE, Llewellin EW, Watkins JM, Befus KS (2017) Formation of obsidian pyroclasts by sintering of ash particles in the volcanic conduit. Earth Planet Sci Lett 459:252–263

Gardner JE, Wadsworth FB, Llewellin EW, Watkins JM, Coumans JP (2018) Experimental sintering of ash at conduit conditions and implications for the longevity of tuffisites. Bull Volcanol 80:23

Gardner JE, Wadsworth FB, Llewellin EW, Watkins JM, Coumans JP (2019) Experimental constraints on the textures and origin of obsidian pyroclasts. Bull Volcanol 81(4):22

Gonnermann HM, Manga M (2005a) Nonequilibrium magma degassing: results frommodeling of the ca. 1340 AD eruption of mono craters, California. Earth Planet Sci Lett 238(1):1–16

Gonnermann HM, Manga M (2005b) Flow banding in obsidian: a record of evolving textural heterogeneity during magma deformation. Earth Planet Sci Lett 236(1):135–147

Hammer JE, Cashman KV, Hoblitt RP, Newman S (1999) Degassing and microlite crystallization during pre-climactic events of the 1991 eruption of Mt. Pinatubo, Philippines. Bull Volcanal 60(5):355–380

Hess K-U, Dingwell DB (1996) Viscosities of hydrous leucogranitic melts: a non-Arrhenian model. Am Mineral 81:1297–1300

Hoblitt RP, Wolfe EW, Scott WE, Couchman MR, Pallister JS, Javier D (1996) The preclimactic eruptions of Mount Pinatubo, June 1991. Fire and Mud: eruptions and lahars of Mount Pinatubo, Philippines, pp 457–511

Kolzenburg S, Ryan AG, Russell JK (2019) Permeability evolution during non-isothermal compaction in volcanic conduits and tuffisite veins: implications for pressure monitoring of volcani edifices. Earth Planet Sci Lett 527:115783

Liu Y, Zhang Y, Behrens H (2005) Solubility of H_2O in rhyolitic melts at low pressure and a new empirical model for mixed H_2O-CO_2 solubility in rhyolitic melts. J Volcanol Geotherm Res 143:219–235

Luhr JF, Melson WG (1996) Mineral and glass compositions in June 15, 1991, pumices: evidence for dynamic disequilibrium in the dacite of Mount Pinatubo. Fire and Mud: Eruptions and Lahars of Mount Pinatubo, Philippines, 733–750

Martel C, Iacono-Marziano G (2015) Timescales of bubble coalescence, outgassing, and foam collapse in decompressed rhyolitic melts. Earth Planet Sci Lett 412:173–185

Newman S, Epstein S, Stolper E (1988) Water, carbon dioxide and hydrogen isotopes in glasses from the ca. 1340 A.D. eruption of the Mono Craters, California: constraints on degassing phenomena and initial volatile content. J Volcanol Geotherm Res 35:75–96

Pallister JS, Hoblitt RP, Reyes AG (1992) A basalt trigger for the 1991 eruptions of Pinatubo volcano? Nature 356:426–428

Pallister JS, Hoblitt RP, Meeker GP, Knight RJ, Siems DF (1996) Magma mixing at Mount Pinatubo: petrographic and chemical evidence from the 1991 deposits. Fire and mud: eruptions and lahars of Mount Pinatubo, Philippines, pp 687–731

Polacci M, Papale P, Rosi M (2001) Textural heterogeneities in pumice from the climactic eruptions of Mount Pinatubo, 15 June 1991, and implications for magma ascent dynamics. Bull Volcanol 63:83–97

Proussevitch AA, Sahagian DL, Kutolin VA (1993) Stability of foams in silicate melts. J Volcanol Geotherm Res 59(1–2):161–178

Rust AC, Cashman KV (2007) Multiple origins of obsidian pyroclasts and implications for changes in the dynamics of the 1300 B.P. eruption of Newberry Volcano, USA. Bull Volcanol 69:825–845

Rust AC, Manga M (2002) Bubble shapes and orientations in low re simple shear flow. J. Colloid Interface Sci 249:476–480

Rust AC, Cashman KV, Wallace PJ (2004) Magma degassing buffered by vapor flow through brecciated conduit margins. Geology 32: 349–352

Rutherford MJ, Devine JD (1996) Preeruption pressure-temperature conditions and volatiles in the 1991 dacitic magma of Mount Pinatubo. Fire and mud: eruptions and lahars of Mount Pinatubo, Philippines, pp 751–766

Scaillet B, Evans BW (1999) The 15 June 1991 eruption of mount Pinatubo. I. Phase Equilibria and pre-eruption $P–T–fO_2–fH_2O$ conditions of the dacite magma. J Petrol 40:381–411

Scott WE, Hoblitt RP, Torres RC, Self S, Martinez ML, Nillos T Jr (1996) Pyroclastic flows of the June 15, 1991, climactic eruption of Mount Pinatubo. Fire and mud: eruptions and lahars of Mount Pinatubo, Philippines, pp 545–570

Self S, Wilson L, Nairn IA (1979) Vulcanian eruption mechanisms. Nature 277(5696):440–443

Taylor GI (1934) The formation of emulsions in definable fields of flow. Proc R Soc Lond Ser A146:501–523

Taylor BE, Eichelberger JC, Westrich HR (1983) Hydrogen isotopic evidence of rhyolitic magma degassing during shallow intrusion and eruption. Nature 306:541–545

Wadsworth FB, Vasseur J, Llewellin EW, Schauroth J, Dobsan KJ, Scheu B, Dingwell DB (2016) Sintering of viscous droplets under surface tension. Proc R Soc A 472:20150780

Wadsworth FB, Vasseur J, Llewellin EW, Dobsan KJ, Colombier M, von Aulock FW, Fife JL, Wiesmaier S, Hess K-U, Scheu B, Lavallée Y, Dingwell DB (2017a) Topological inversions in coalescing granular media control fluid-flow regimes. Phys Rev E 96:033113

Wadsworth FB, Vasseur J, Llewellin EW, Dingwell DB (2017b) Sintering of polydispersive viscous droplets. Phys Rev E 95:033114

Wadsworth FB, Llewellin EW, Vasseur J, Gardner JE, Tuffen H (2020) Explosive-effusive volcanic eruptions transitions caused by sintering. Sci Adv 6:eaba7940

Wallace P, Gerlach TM (1994) Magmatic vapour source for sulfur dioxide released during volcanic eruptions: evidence from Mount Pinatubo. Science 265:497–499

Watkins JM, Gardner JE, Befus KS (2017) Nonequilibrium degassing, regassing, and vapor fluxing in magmatic feeder systems. Geology 45(2):183–186

Weisner MG, Wetzel A, Catane SG, Listanco EL, Mirabueno HT (2004) Grain size, areal thickness distribution and controls on sedimentation of the 1991 Mount Pinatubo tephra layer in the South China Sea. Bull Volcanol 66:226–242

Wolfe EW, Hoblitt RP (1996) Overview of the eruptions. Fire and Mud: eruptions and lahars of Mount Pinatubo, Philippines, pp 3–20

Woods AW (1995) A model of vulcanian explosions. Nucl Eng Des 155(1–2):345–357

Wright HMN, Cashman KV, Rosi M, Cioni R (2007) Breadcrust bombs as indicators of Vulcanian eruption dynamics at Guagua Pichincha volcano, Ecuador. Bull Volcanol 69:281–300

Zhang Y, Belcher R, Ihinger PD, Wang L, Xu Z, Newman S (1997) New calibration of infrared measurement of dissolved water in rhyolitic glasses. Geochim Cosmochim Acta 61:3089–3100